One-Dimensional Variational Retrievals from SSMIS-Simulated Observations

GODELIEVE DEBLONDE

Meteorological Service of Canada, Dorval, Quebec, Canada

STEPHEN ENGLISH

Met Office, Bracknell, Berkshire, United Kingdom

(Manuscript received 15 November 2002, in final form 23 March 2003)

ABSTRACT

Retrievals using synthetic background fields and observations for the Special Sensor Microwave Imager Sounder (SSMIS) instrument are performed using a one-dimensional variational data assimilation (1DVAR) scheme for clear and cloudy nonprecipitating skies over open oceans. Two retrieval techniques are implemented in the 1DVAR and are extensively tested. Profiles of temperature, marine surface wind speed, and skin temperature are retrieved with both techniques. In addition, with technique A, profiles of the natural logarithm of specific humidity and liquid water path are also retrieved. With technique B, the natural logarithm of total water content (sum of specific humidity and liquid cloud water content) is retrieved instead of the natural logarithm of humidity and liquid water path. A function specifies how total water content is split among its two components. In essence, excess water vapor oversaturation leads to cloud formation. Retrievals in clear and cloudy conditions for a variety of experiments thoroughly demonstrate how technique A works. The choice of humidity control variable, the presence of biases in the moisture retrievals, and the impact of applying a supersaturation constraint are also discussed. Furthermore, in the presence of clouds, it is shown that little temperature information can be extracted with this technique if the a priori cloud vertical distribution is not known well. With technique B, however, temperature information can be extracted from the observations even in the presence of clouds. Because of its more physically based parameterization, it has some skill at positioning the cloud in the vertical direction.

1. Introduction

A stand-alone one-dimensional variational data assimilation (1DVAR) scheme is developed to compute retrievals from the Defense Meteorological Satellite Project (DMSP) Special Sensor Microwave Imager Sounder (SSMIS) brightness temperature. The SSMIS (scheduled for launch in October 2003) is designed to measure profiles of humidity, temperature, surface properties (such as marine surface wind speed), and cloud liquid water path. This instrument is a follow on to the combination of the Special Sensor Microwave Imager (SSM/I), Special Sensor Microwave Temperature Sounder (SSM/T1), and Special Sensor Microwave Water Vapor Sounder (SSM/T2) instruments. However, the SSMIS also has channels that measure temperature in the mesosphere.

The 1DVAR can also compute retrievals from the National Oceanic and Atmospheric Administration (NOAA) Advanced Microwave Sounding Unit (AMSU)-A/B instruments, which are designed for temperature and moisture sounding. The SSMIS and AMSU-A/B instruments have several channels that are very similar, but have different scanning properties. The former maintains a fixed nadir view angle along a scan (conical scan), while the latter scans across track.

The 1DVAR can be solved using two different approaches. The first approach, based on Phalippou (1996), retrieves profiles of humidity and temperature, surface wind speed, liquid water path, and skin temperature. The second approach consists of retrieving total water content (sum of water vapor and cloud liquid water content) profiles instead of profiles of humidity and liquid water path. An empirical function governs how the total water content is split among its two components. In essence, cloud water is allowed to form when the atmospheric relative humidity (RH) has reached a preset threshold value.

The second approach has similarities to the retrieval schemes presented in Rosenkranz (2001) and Blankenship et al. (2000). Rosenkranz (2001) designed a retrieval scheme for the AMSU-A/B instruments. Humidity and temperature retrievals are solved for sequentially and each use a different subset of channels. Humidity

Corresponding author address: Dr. Godelieve Deblonde, Meteorological Service of Canada, 2121 Trans-Canada Highway, Dorval, QC H9P 1J3, Canada.
E-mail: godelieve.deblonde@ec.gc.ca

retrievals are obtained from AMSU-A window channels (1, 2, 3, and 15) and AMSU-B humidity sounding channel (183 GHz), while temperature retrievals are obtained from AMSU-A channels 4–14, which are only sensitive to temperature. For the 1DVAR approaches presented here, retrievals are obtained using all channels at once. Other differences involve convergence criteria of the iterative procedure and the a priori values of the retrieved variables. For the 1DVAR, a priori values are intended to be provided by short-term forecasts, which are also referred to as background fields. In Rosenkranz (2001), they are obtained from previously collected datasets for temperature and a global value is used for RH.

Blankenship et al.'s (2000) retrieval scheme, based on that developed by Wilheit (1990), computes profiles of humidity from SSM/I-integrated water vapor (obtained from a regression equation) and brightness temperature from the SSM/T2 183-GHz channels. The authors also explore the use of the natural logarithm of RH, as opposed to RH itself, as a humidity control variable to reduce the nonlinear dependence on humidity of the optical depth for those channels that sample the 183-GHz absorption line.

The 1DVAR presented here uses realistic modeling of the apparent surface temperature of the oceans. The main reasons for using simulated data in this study are 1) that it allows for a thorough testing and a more complete understanding of the retrieval scheme, and 2) that the satellite launch carrying the SSMIS instrument is pending. The 1DVAR methodology is presented in section 2. Results of retrievals with simulated data in clear skies are presented in section 3. This section also discusses the impact of using a supersaturation constraint and the presence of biases in the moisture retrievals. Results are also shown for a case where an attempt is made to remove these biases by first removing the biases between the observed and forward-modeled brightness temperature (T_b) as might be done in an operational application of the 1DVAR. In section 4, synthetic clouds are included in the simulated fields. With technique A, the impact of the supersaturation constraint and that of the a priori knowledge of the cloud vertical distribution are investigated. With technique B, it is shown that temperature information can also be extracted because the technique has some skill at positioning the cloud in the vertical. Conclusions are given in section 5.

2. 1DVAR methodology

The control variables of the 1DVAR are either (a) profiles of temperature, profiles of the natural logarithm of specific humidity (ln$q$), marine surface wind speed, and cloud liquid water path (LWP), or (b) profiles of temperature, profiles of the natural logarithm of total water content, and marine surface wind speed. Total water content is the sum of specific humidity and cloud liquid water content. For both cases, the skin temperature can optionally also be solved for. The retrieval technique using the first set of control variables will be referred to as technique A, and the second set as technique B.

a. 1DVAR analysis system

The a priori or background information of the atmosphere and surface ($\mathbf{x}^b$), and the measurements $\mathbf{Tb}^o$ (observed brightness temperature) are combined in a statistically optimal way to obtain an estimate of the most probable atmospheric state $\mathbf{x}$. It is assumed that the error distribution for both $\mathbf{x}^b$ and $\mathbf{Tb}^o$ is Gaussian with zero mean and that the background and observation error is uncorrelated. The most probable state is obtained by minimizing the cost function $J(\mathbf{x})$ (e.g., Lorenc 1986), which may be written as

$$J(\mathbf{x}) = \frac{1}{2}(\mathbf{x} - \mathbf{x}^b)\mathbf{B}^{-1}(\mathbf{x} - \mathbf{x}^b)^{\mathrm{T}} + \frac{1}{2}[\mathbf{Tb}^o - H(\mathbf{x})](\mathbf{E} + \mathbf{F})^{-1}[\mathbf{Tb}^o - H(\mathbf{x})]^{\mathrm{T}}, \quad (1)$$

where $\mathbf{B}$, $\mathbf{E}$, and $\mathbf{F}$ are, respectively, the background, instrument, and representativeness (includes forward-modeling error) error covariance matrices. The superscripts T and -1 denote transpose and inverse, respectively. The observation operator that simulates brightness temperature is $H(\mathbf{x})$.

The Levenberg–Marquardt technique (Press et al. 1986) is used to find the minimum of the cost function. This technique is well suited for problems where $H(\mathbf{x})$ is nonlinear, as is the case here (e.g., Rodgers 2000), and is a combination of a Gauss–Newton and steepest descent minimization technique. Convergence criteria also follow Press et al. (1986).

1) TECHNIQUE A: RETRIEVAL OF LNQ AND LWP

Phalippou (1996) developed a 1DVAR for the SSM/I instrument, which has channels that are similar to SSMIS channels 12–18 (see Table 1). The brightness temperature of these window channels has little sensitivity to where the cloud is located in the vertical. His 1DVAR has been used operationally both at the European Centre for Medium-Range Weather Forecasts (Gérard and Saunders 1999) and at the Met Office. Technique A is an extension of this 1DVAR because profiles of temperature and skin temperature are also solved for. The control vector consists of a profile of temperature (T, at 43 vertical levels $\geq$0.1 hPa), a profile of ln$q$, at 22 vertical levels below 200 hPa), marine surface wind speed (SWS), and LWP. LWP is the integral with respect to pressure p of the cloud liquid water content $q_L(p)$ divided by the gravitational constant. To constrain the supersaturation of water vapor, a weak constraint is added to $J(\mathbf{x})$ [Eq. (1)], and is defined as follows:

TABLE 1. SSMIS channel parameter specifications—RF: radio frequency; V: vertical polarization; H: horizontal polarization; RC: right circular polarization.

Channel No.	Frequency* (GHz)	RF bandwidth (MHz)	Polarization	3-dB footprint (km)**	Sample spacing (km)**	NEΔT at 305 K (K)
1	50.3	380.0	H	37.7 × 38.8	37.5	0.21
2	52.8	388.8	H	37.7 × 38.8	37.5	0.20
3	53.596	380.0	H	37.7 × 38.8	37.5	0.21
4	54.40	382.5	H	37.7 × 38.8	37.5	0.20
5	55.50	391.3	H	37.7 × 38.8	37.5	0.22
6	57.29	330.0	RC	37.7 × 38.8	37.5	0.26
7	59.4	238.8	RC	37.7 × 38.8	37.5	0.25
8	150.0 ± 1.25	3284.0	H	13.2 × 15.5	12.5	0.53
9	183.31 ± 6.6	1025.0	H	13.2 × 15.5	12.5	0.56
10	183.31 ± 3.0	2038.0	H	13.2 × 15.5	12.5	0.39
11	183.31 ± 1.0	3052.0	H	13.2 × 15.5	12.5	0.38
12	19.35	355.0	H	46.5 × 73.6	25	0.35
13	19.35	356.7	V	46.5 × 73.6	25	0.34
14	22.235	407.5	V	46.5 × 73.6	25	0.45
15	37.0	1615.0	H	31.2 × 45.0	25	0.26
16	37.0	1545.0	V	31.2 × 45.0	25	0.22
17	91.655 ± 0.9	2836.0	V	13.2 × 15.5	12.5	0.19
18	91.655 ± 0.9	2822.0	H	13.2 × 15.5	12.5	0.19
19	63.283 248 ± 0.285 271	2.72	RC	75.2 × 75.0	75	1.23
20	60.792 668 ± 0.357 892	2.70	RC	75.2 × 75.0	75	1.18
21	60.792 668 ± 0.357 892 ± 0.002	5.16	RC	75.2 × 75.0	75	0.86
22	60.792 668 ± 0.357 892 ± 0.0055	10.48	RC	75.2 × 75.0	75	0.58
23	60.792 668 ± 0.357 892 ± 0.016	29.28	RC	75.2 × 75.0	75	0.37
24	60.792 668 ± 0.357 892 ± 0.050	106.0	RC	37.7 × 38.8	37.5	0.38

* Center frequency ± first IF ± second IF (IF = intermediate frequency).
** Assumes spacecraft altitude of 833 km.

$$J_{\text{sat}} = \begin{cases} a(\ln q - \ln q_{\text{sat}})^3; & q > q_{\text{sat}} \\ 0; & q \le q_{\text{sat}}, \end{cases} \quad (2)$$

where q_{sat} is the specific humidity at saturation and a is an empirical constant ($a = 4000.0$). During the minimization process of $J(\mathbf{x})$, LWP is allowed to vary while the cloud structure function (CSF) is maintained fixed. CSF is defined as

$$\text{CSF}(p) = q_L^b(p)/\text{LWP}^b, \quad (3)$$

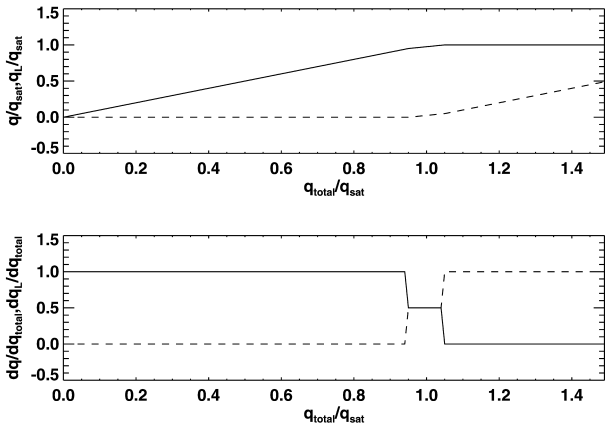

FIG. 1. (a) Dependence of q/q_{sat} and q_L/q_{sat} on $q_{\text{total}}/q_{\text{sat}}$ ($q_{\text{total}} = q + q_L$) and (b) derivatives of q (continuous line) and q_L (dashed line) with respect to q_{total} as a function of $q_{\text{total}}/q_{\text{sat}}$.

where the superscript b denotes background fields. The term q_L is computed from the retrieved LWP as follows:

$$q_L(p) = \text{CSF}(p)\text{LWP}. \quad (4)$$

When LWP^b is zero, CSF is as defined in appendix A.

2) TECHNIQUE B: RETRIEVAL OF LNq_{total}

The control variables for technique B are the same as those of technique A, except that instead of solving for ln$q$ and LWP, one solves for the natural logarithm of total water content lnq_{total} where $q_{\text{total}} = q + q_L$. Prior to computing $H(\mathbf{x})$, q_{total} is split among its water vapor content and cloud liquid water content with an empirical function (Fig. 1, appendix B). Cloud water is allowed to form when the atmospheric relative humidity reaches the preset threshold value of 95%.

b. Radiative transfer model

Brightness temperature is computed with the fast radiative transfer model called Rapid Transmittance TIROS Operational Vertical Sounder (RTTOV), (e.g., Eyre 1991; Saunders et al. 1999) version 6.7. This version was adapted by the first author of this paper for the SSMIS instrument. The optical depth regression equations are developed from a line-by-line absorption model based on Liebe (1989) for water vapor absorption and Liebe et al. (1992) for oxygen absorption. The

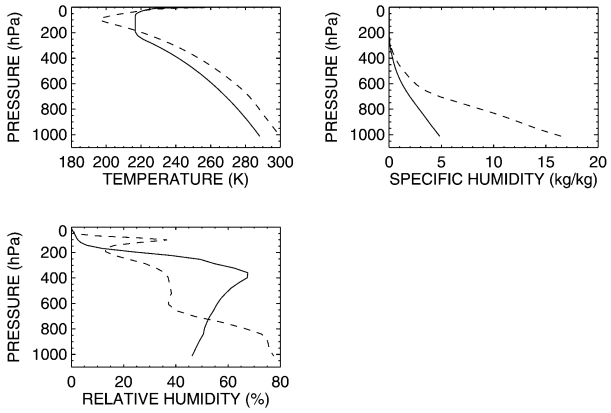

FIG. 2. True profiles used for simulating background and observed fields: *U.S. Standard Atmosphere, 1976* profile (USSD) with IWV = 14.2 kg m^{-2} (continuous line) and tropical profile (TROP) with IWV = 41.3 kg m^{-2} (dashed line).

RTTOV fast surface emissivity model is FASTEM2 (English and Hewison 1998; Deblonde and English 2000). This model employs regression equations obtained from a much slower geometric optics model (e.g., Petty and Katsaros 1994). RTTOV can not simulate brightness temperature in the presence of precipitation because scattering effects are not included.

c. SSMIS instrument

The SSMIS channel characteristics are listed in Table 1. The SSMIS is a conical scanner with a fixed nadir view angle of 45°. Further information may be found in Swadley and Chandler (1991) and Bommarito (1993). Channels whose weighting functions peak above 0.1 hPa (i.e., channels 19, 20, and 21) are ignored here because the application of the 1DVAR is in the troposphere and stratosphere. The Zeeman effect is included in a simplified way (Liebe 1989) and affects mostly channel 22, which is the highest peaking channel of the remaining channels.

d. Simulation of background fields and observations

To test the 1DVAR scheme, numerous retrievals are performed using both simulated background fields and brightness temperature. This approach, which offers the advantage of knowing the true solution, follows that of Eyre (1989) and is described in appendix C. Two true profiles ($\mathbf{x}^{\text{true}}$) are selected: the *U.S. Standard Atmosphere, 1976* and a tropical atmosphere, and are illustrated in Fig. 2. The integrated water vapor (IWV) of the profiles are, respectively, 14.2 and 41.3 kg m^{-2}. These profiles are meant to represent midlatitude dry and moist conditions. Both profiles have SWS = 7 m s^{-1}. Observed brightness temperature $\mathbf{Tb}^o$ is simulated as follows:

$$\mathbf{Tb}_k^o = \mathbf{Tb}_k(\mathbf{x}^{\text{true}}) + N(0, \sigma_k) \quad (5)$$

TABLE 2. SSMIS $(\mathbf{E} + \mathbf{F})^{1/2}$ values (K) (section 2).

Channel	$(\mathbf{E} + \mathbf{F})^{1/2}$	Channel	$(\mathbf{E} + \mathbf{F})^{1/2}$
1	1.5	12	2.4
2	0.4	13	1.27
3	0.4	14	1.44
4	0.4	15	3.00
5	0.4	16	1.34
6	0.4	17	1.74
7	0.4	18	3.75
8	3.0	22	0.64
9	3.0	23	0.46
10	3.0	24	0.47
11	3.0		

The index k denotes channel number and σ_k equals $(\mathbf{E} + \mathbf{F})^{1/2}$ whose values are listed in Table 2. Here N is a normal distribution with mean zero and variance σ_k^2.

Clouds to be added to the selected true profile are created by first generating a CSF as described in appendix A. Subsequently, CSF is multiplied by the desired value of LWP. For technique A, at levels where clouds are to be added to the true profile, the specific humidity of the true profile is replaced with its saturated value. All samples of the simulated background field have the same cloud profile as that of the true profile. For technique B, the specific humidity of the true profile is saturated to only 95% at levels where clouds will be added. If the saturation level were higher, then clouds would be formed by the saturation step (appendix B). Clouds are only added after the saturation step. Cloud profiles of the background fields are determined using the splitting functions and vary from one profile to another because noise (appendix C) is added to the true profile of total water content $\ln q_{\text{total}}^{\text{true}}$.

e. Background and observation error

Background covariance error ($\mathbf{B}$) for profiles of T and $\ln q$, air temperature and $\ln q$ at 2 m, and skin temperature (T_{skin}) were obtained from the Met Office 1DVAR background error dataset for three different latitudinal bands: Northern Hemisphere, Southern Hemisphere, and the Tropics. Only Northern Hemisphere errors are used in this study. Errors for other latitudinal bands are shown for comparison. The background error standard deviation of T and $\ln q$ are illustrated in Fig. 3. To reflect oceanic values, T_{skin} background error is replaced with 0.9 K (Northern Hemisphere band). Over the oceans, it is assumed that the skin temperature is equal to the sea surface temperature. The background error of $\ln q$ at 2 m is taken to be that of the lowest $\ln q$ level (level 43). Covariance error between T and $\ln q$ is set to zero (univariate analysis). For SWS background error, a value of 2 m s^{-1} is used. For technique A, the LWP background error is set to 0.2 kg m^{-2}. Such a large error value implies that the LWP is unconstrained by the background. For technique B, $\ln q_{\text{total}}$ is assigned the same background error as $\ln q$ for lack of a better knowledge.

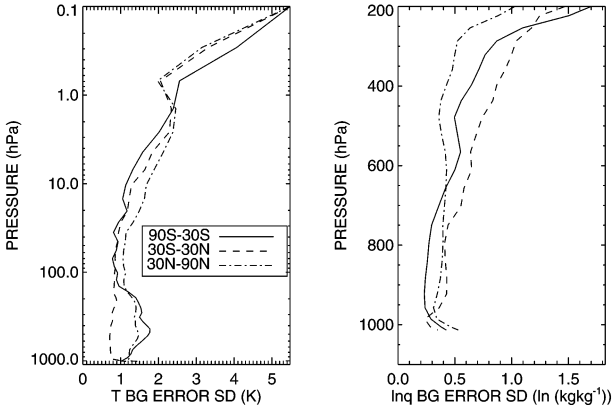

FIG. 3. Met Office 1DVAR (left) temperature and (right) ln$q$ background error standard deviations (square root of the diagonal elements of the **B** matrix) for three different latitude bands: 90°–30°S or Southern Hemisphere, 30°S–30°N or Tropics, and 30°–90°N or Northern Hemisphere.

The background error of the atmospheric surface pressure is set to 1 hPa for all cases.

Errors for observations $(\mathbf{E} + \mathbf{F})^{1/2}$ are listed in Table 2. The errors for channels 12–18 (SSM/I-like channels) and channels 8–11 (similar to SSM/T2 channels) are taken from Deblonde (2001) and are based on observation minus forecast (6-h forecast brightness temperature computed with RTTOV) statistics of brightness temperature. For the remaining channels, error estimates are based on English (1999).

f. Definitions of statistics and normalized errors

In the linear limit of the forward model $H(\mathbf{x})$, the inverse of the analysis error covariance matrix **A** is given by (e.g., Rodgers 2000)

$$\mathbf{A}^{-1} = J''(\mathbf{x}) = \mathbf{B}^{-1} + H'(\mathbf{x}_n)(\mathbf{E} + \mathbf{F})^{-1}H'(\mathbf{x}_n), \quad (6)$$

where $H'(\mathbf{x})$ is the Jacobian of $H(\mathbf{x})$. Note that in the above equation, the Hessian $[J''(\mathbf{x})]$ is computed at the solution value $\mathbf{x}_n$ (i.e., once the solution has reached convergence). In this paper, we will refer to the square root of the diagonal elements of **A** as the ''theoretical'' error and the computed error will be the error between the true profiles and the solution $\mathbf{x}_n$.

For a given $y = x_1 - x_2$, bias$(x_1 - x_2)$ and SD$(x_1 - x_2)$ are defined as follows:

$$\text{bias}(y) = \frac{1}{N}\sum_{i=1}^{N} y_i \qquad \text{and} \quad (7)$$

$$\text{SD}(y) = \sqrt{\frac{1}{N-1}\sum_{i=1}^{N}(y_i - \overline{y})^2}, \quad (8)$$

where i is the sample number.

The normalized computed error (NCE) and the normalized theoretical error (NTE) at level j are, respectively, defined as

$$\text{NCE}_j = \frac{\text{SD}[\mathbf{x}_n(p_j) - \mathbf{x}^{\text{true}}(p_j)]}{B_{jj}^{1/2}} \qquad \text{and} \quad (9)$$

$$\text{NTE}_j = \frac{A_{jj}^{1/2}}{B_{jj}^{1/2}}, \quad (10)$$

where **A** is as defined in Eq. (6) and B_{jj} are the diagonal elements of **B**.

3. SSMIS retrievals in cloudless skies

a. Retrievals with technique A

The 1DVAR is solved using, as true profiles, the tropical and *U.S. Standard Atmosphere, 1976* cloudless profiles (Fig. 2) experiments NCA1 and NCA2, respectively (see Table 3 for the naming convention for the experiments). With the background and observation error as specified, very low values of NCE (0.160 and 0.263) are obtained for IWV. This indicates a very large impact of the observations because the solution error is much lower than the background error. Several of the SSMIS window channels (low optical depth) are very sensitive to IWV. Assimilating SSMIS T_b does not pro-

TABLE 3. Description of experiments. Experiment naming convention: no cloud (NC) or cloud (C) followed by retrieval technique A or B, and experiment number; tropical true profile: TROP; *U.S. Standard Atmosphere, 1976* profile: USSD; supersaturation constraint: SSC; background: BG; relative humidity: RH; and cloud structure function: CSF. Pressure: hPa; LWP: kg m^{-2}.

Expt	Retrieval technique	True profile	Cloud in profile	Cloud-top and -bottom pressure, LWP	Comment
NCA1	A	TROP	NO	N/A	
NCA2	A	USSD	NO	N/A	
NCA3	A	TROP	NO	N/A	As NCA1 but bias removed
NCB4	B	TROP	NO	N/A	As NCA1 but with technique B
NCB5	B	USSD	NO	N/A	As NCA2 but with technique B
CA6	A	USSD	YES	700–750, 0.3	With SSC, CSF from BG cloud
CA7	A	USSD	YES	700–750, 0.3	Without SSC, CSF from BG cloud
CA8	A	USSD	YES	700–750, 0.3	As CA6, but CSF from BG RH
CA9	A	USSD	YES	750–950, 0.5	With SSC, CSF from BG cloud
CA10	A	USSD	YES	750–950, 0.5	As CA9, but CSF from BG RH
CB11	B	TROP	YES	700–750, 0.267	
CB12	B	TROP	YES	750–950, 0.187	

TABLE 4. Bias and SD for $\mathbf{x} - \mathbf{x}^{\text{true}}$ and NCE for experiments without clouds. IWV and LWP: kg m^{-2}, SWS: m s^{-1}. Sample size = 3000; BG: background. Northern Hemisphere background error is used for all experiments. For each experiment, top number is bias($\mathbf{x} - \mathbf{x}^{\text{true}}$) and bottom number is SD($\mathbf{x} - \mathbf{x}^{\text{true}}$) as defined in section 2f.

Expt	True profile (No. of diverging cases)	Normalized computed error			IWV		LWP		SWS	
		IWV	SWS	T_{skin}	1DVAR solution	BG	1DVAR solution	BG	1DVAR solution	BG
NCA1	TROP (3)	0.160	0.762	0.944	0.083	3.153	−0.004	0.000	0.010	−0.024
					1.562	9.769	0.038		1.506	1.975
NCA2	USSD (7)	0.263	0.701	0.958	0.040	1.088	−0.002	0.000	0.009	−0.020
					0.844	3.213	0.015		1.385	1.975
NCB4	TROP (263)	—	0.750	0.946	−0.379	0.305	0.026	1.775	−0.014	−0.033
					1.250	6.749	0.047	2.740	1.497	1.996
NCB5	USSD (339)	—	0.691	0.967	−0.222	0.757	0.011	0.264	−0.148	−0.071
					0.603	2.832	0.015	0.632	1.389	2.009
NCA3	TROP (1)	0.166	0.793	0.968	2.419	3.152	0.019	0.000	0.342	−0.023
					1.625	9.767	0.040		1.566	1.975

vide much information on T_{skin} (Table 4). The values of its background error is low over the oceans (section 2e) and the dependence of T_b on T_{skin} is low. The information provided by the observations on SWS is considerable: NCE = 0.762 and 0.701. All retrieval results presented in this paper are for situations where the surface is an open ocean. If retrievals were performed over land for instance, then information would be extracted from the T_b because the skin temperature background error over land is considerably larger than that over the open oceans.

The square root of the diagonal elements of the matrix $\mathbf{B}$ and SD($\mathbf{x}^b - \mathbf{x}^{\text{true}}$) are illustrated in Fig. 4a for T and Fig. 4c for ln$q$. If the background field is simulated correctly, then these two curves should overlap. This is the case within numerical accuracy. Biases and SD for background and solution fields with respect to the true solution are also illustrated in the same figures.

NCE and NTE are illustrated in Fig. 4b for T and Fig. 4d for ln$q$. If $H(\mathbf{x})$ is linear, then NCE should be the same as NTE. NCE and NTE are close for T. This is expected because the dependence of T_b on T is very

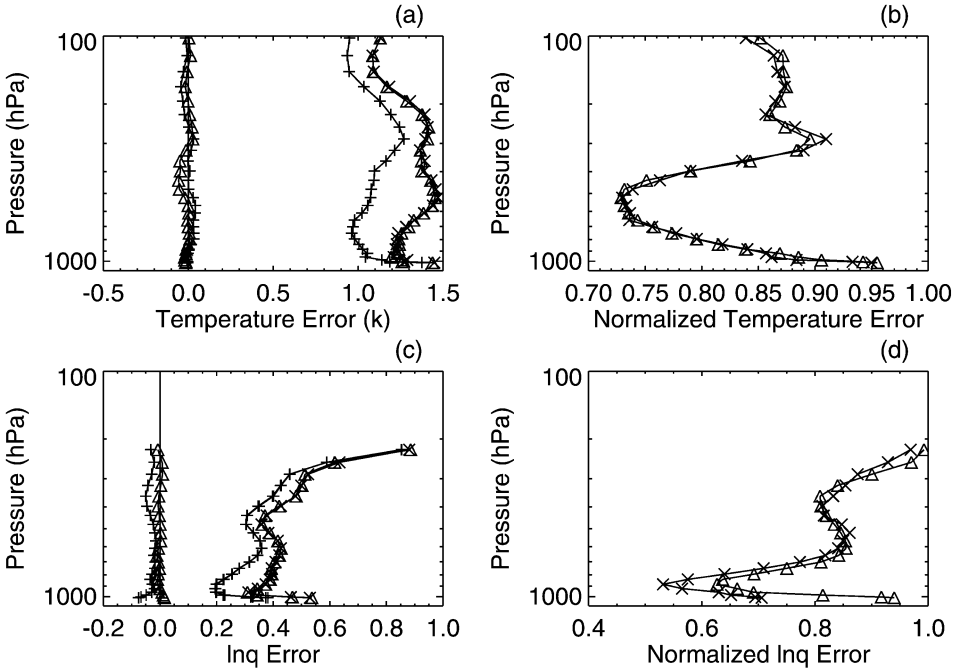

FIG. 4. Temperature and ln$q$ profile retrieval errors for a cloudless true tropical profile for experiment NCA1. (a) Bias (left of figure) and SD (right of figure) of ($T^b - T^{\text{true}}$) (curves with triangles), bias and SD of ($T^{\text{sol}} - T^{\text{true}}$)(curves with plus signs). The superscript sol denotes the 1DVAR solution. Square root of the diagonal elements of $\mathbf{B}$ (curves labeled with x), (b) Temperature normalized computed error (x signs) and normalized theoretical error (triangles), (c) same as in (a), but for ln$q$, and (d) same as in (b) but for ln$q$.

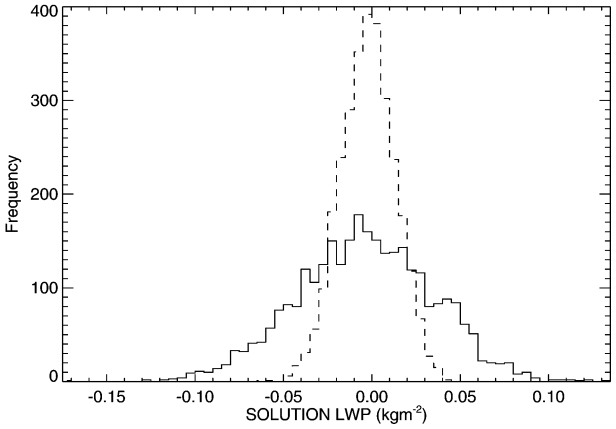

FIG. 5. Histograms of cloud liquid water path (kg m^{-2}) for experiments NCA1 (continuous line) and NCA2 (dashed line).

close to linear, and in particular, for channels that only depend on temperature (channels 3–7, 22–24). However, this is not the case for ln$q$ because its dependence on T_b is nonlinear. Small differences in the NCE and NTE curves (Fig. 4d) for the upper levels are partly due to the fact that background humidity is cut off to a minimum value (3×10^{-6} kg kg^{-1}). As a result, the background ln$q$ distribution is slightly skewed. The supersaturation constraint (SSC) [Eq. (2)] also contributes to the differences. An experiment in which the SSC is removed (not shown here) has NCE and NTE much closer below ~600 hPa. Addition of the SSC provides a solution closer to the true one, because NCE is smaller than NTE for levels below ~600 hPa. The nonlinearity of the 1DVAR problem can be reduced by reducing the size of the elements of **B** (e.g., Eyre and Collard 1999) and should result in the two curves being close to each other. This is indeed found to be the case for the 1DVAR described here.

As shown in Fig. 4c, bias(lnq^{sol} − lnq^{true}) is not zero for all heights (the superscript sol refers to the 1DVAR solution), but bias(IWV$^{\text{sol}}$ − IWV$^{\text{true}}$) for experiments NCA1 and NCA2 is very small (Table 4). Several of the SSMIS window channels have a large dependence on IWV and SSMIS T_b essentially control the value of IWV$^{\text{sol}}$. The solution humidity bias is further discussed in section 3c. Statistics for LWP$^{\text{sol}}$ are also listed in Table 4. The SD(LWP$^{\text{sol}}$ − LWP$^{\text{true}}$) is larger for the tropical profile than for the *U.S. Standard Atmosphere, 1976* profile, which is much drier. Histograms of LWP$^{\text{sol}}$ for NCA1 and NCA2 are illustrated in Fig. 5. Both negative and positive values of LWP$^{\text{sol}}$ are obtained. The SSMIS channels are not sensitive to very low values of LWP and, hence, Gaussian noise added to the true T_b [to simulate the observed T_b, see, Eq. (5)] leads to retrievals of both signs. The size of the LWP retrieval error obtained is of the expected magnitude (e.g., Greenwald et al. 1993; Alishouse et al. 1990). It should be noted that a large background error is assigned to LWP and, hence, the background LWP does not influence the solution. In the limit when LWP^b error is set to very small, no clouds are generated.

b. Retrievals with technique B

For technique B, lnq_{total} is the control variable instead of ln$q$ and LWP. The 1DVAR problem now also implicitly includes a SSC: when saturation is reached, excess water leads to cloud formation by construction (see splitting functions described in appendix B). The problem is also more nonlinear: Eq. (B1) contains sharp transitions. To help with the nonlinearity, the maximum number of iterations is increased from 20 (for technique A) to 30. Furthermore, a maximum value is set for the change $\Delta\mathbf{x}$ brought on to the solution at each iteration (denoted by n) of the minimization where $\mathbf{x}_{n+1} = \mathbf{x}_n + \Delta\mathbf{x}$. For the majority of retrieval cases with technique B, convergence is reached after less than 10 iterations. The number of maximum iterations is set to a high value to maximize the number of converging cases so that as complete a set as is possible can be obtained for the computation of the retrieval statistics.

Experiments NCB4 and NCB5 are the same as experiments NCA1 and NCA2, respectively, except that the moisture control variable is different. The moisture control variable for experiments NCB4 and NCB5 is as described in section 2a(2). The percentage of diverging cases for NCB4 and NCB5 is about 10% (Table 4, second column). The sample size for all experiments is 3000. Note that with technique A, the percentage of diverging cases is close to zero. The statistics listed in Table 4 are computed by excluding diverging cases. Because a nonnegligible number of samples did not converge, the sample set is incomplete and statistics are available for only a subset of the ensemble of profiles. Nevertheless, the retrievals obtained with the two techniques are similar. Figure 6 (technique B) illustrates the same variables as Fig. 4 (technique A), but bias and SD are plotted for lnq_{total} instead of ln$q$ (in Figs. 6c and 6d). Because the retrievals presented in this section are for cloudless true profiles, lnq_{total} and ln$q$ are quite close because the retrieved cloud water content q_L has low values. The SD of IWV^b for NCA1 is larger than that of NCB4 (Table 4). When Gaussian noise is added to the true lnq_{total} profile to generate the background profiles, any water that is in excess of saturation goes toward liquid cloud formation.

LWP retrievals for NCB4 and NCB5 are illustrated in Fig. 7. LWP retrievals with the lnq_{total} formulation can no longer be negative. The distribution of LWP is also considerably smaller for the *U.S. Standard Atmosphere, 1976* profile than for the tropical profile as is the case for technique A. However, for a few of the converging cases, very large values of LWP are retrieved (up to 0.8 kg m^{-2}). For most of these cases, cloud is formed on the lowest pressure level of the profile. This problem could be avoided by prohibiting cloud formation at the surface. For technique A, cloud for-

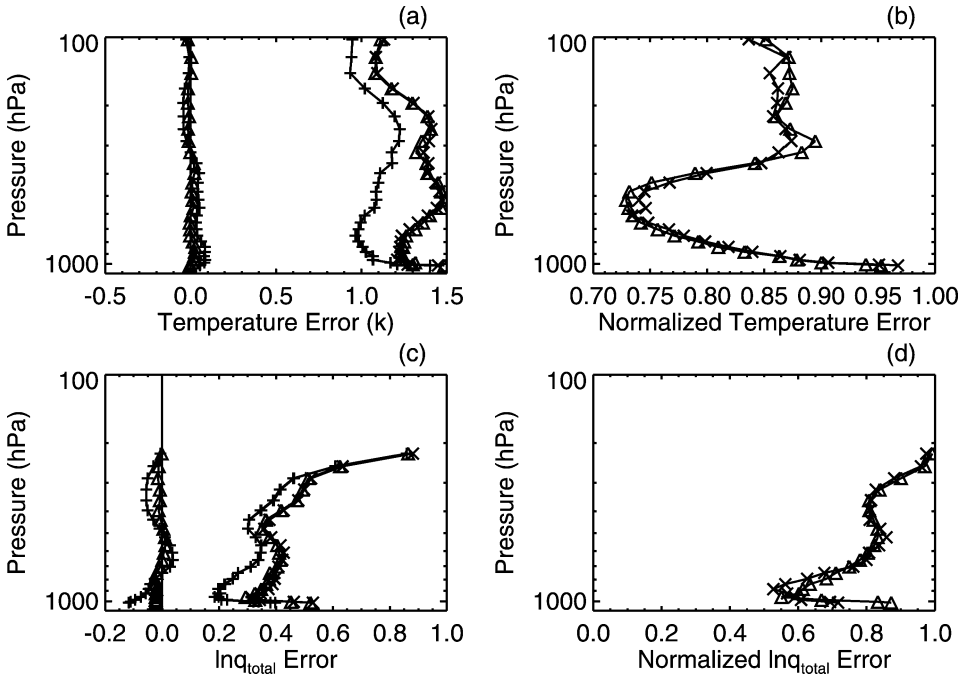

FIG. 6. Same as in Fig. 4, but for experiment NCB4.

mation close to the surface is in fact prohibited (see appendix A).

c. On the solution bias

In the 1DVAR formulation used here, it is assumed that the background error of ln$q$ follows a Gaussian distribution. Hence, the corresponding background error distribution of q is not Gaussian and is skewed. If one simplifies the 1DVAR problem by assuming that ln$q$ is retrieved at a single level, then

$$\ln q^b = \ln q^{\text{true}} + N(0, \sigma_b), \tag{11}$$

and it can be shown that the mean of q^b over the ensemble of profiles is given by

$$\langle q^b \rangle = q^{\text{true}} e^{\sigma_b^2/2}, \tag{12}$$

where $\langle \cdot \cdot \rangle$ indicates an ensemble mean. For $\sigma_b = 0.5$, which is a typical value of ln$q$ background error (Fig. 3), this corresponds to a bias of 13% for $\langle q^b \rangle$ with respect to q^{true}. This is also explains why bias(IWV^b − IWV$^{\text{true}}$) is not zero. IWV is related to q via a linear operator because IWV is simply the integral of q over pressure. Bias(IWV^b − IWV$^{\text{true}}$) for NCA1 (NCA2) is 3.153 (1.088) kg m^{-2} for a true profile IWV value of 41.3 (14.2) kg m^{-2} (Table 4).

For the *U.S. Standard Atmosphere, 1976* true profile experiment (relatively dry profile), assuming that the background error distribution of q is Gaussian rather than that of ln$q$ leads to considerably lower biases between the observations T_b^o and the forward model T_b (computed from the background fields), or $\langle T_b^o - T_b(\mathbf{x}^b) \rangle$. Mean, variance, and skewness of the distribution of $T_b^o - T_b(\mathbf{x}^b)$ for both assumptions are listed in Table 5 for the window channels. The variances of $T_b^o - T_b(\mathbf{x}^b)$ for both assumptions are close, indicating that both distributions have a similar variability as is required for the intercomparison to be valid. The distribution of $T_b^o - T_b(\mathbf{x}^b)$ is considerably more Gaussian (lower values of skewness and visual inspection of the distributions) if the background error of q is assumed Gaussian. This is due to a more linear dependence of the window channels T_b on q rather than ln$q$. When the same assumptions are made for the true tropical profile (larger nonlinear dependence of T_b on moisture), the same conclusion only applies for the few most transparent channels. For the sounding channels, a more Gaussian distribution of $T_b^o - T_b(\mathbf{x}^b)$ is obtained when

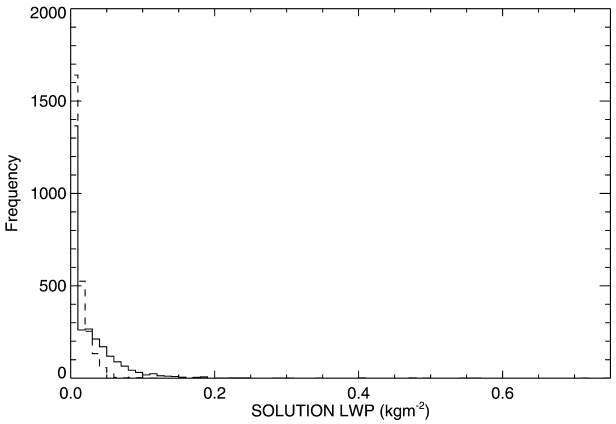

FIG. 7. Histograms of cloud liquid water path (kg m^{-2}) for experiments NCB4 (continuous line) and NCB5 (dashed line).

TABLE 5. The $T_b^o - T_b(\mathbf{x}^b)$ statistics for choosing either a Gaussian distribution for background error of ln$q$ (first entries) or q (second entries).

SSMIS channel No.	Mean	Variance	Skewness
1	−0.67	3.24	−0.95
1	−0.17	2.82	−0.093
12	−1.57	20.42	−0.78
12	−0.16	19.86	0.029
13	−0.82	5.68	−0.800
13	−0.091	5.48	0.016
14	−1.61	22.14	−0.57
14	0.0146	23.93	0.18
15	−1.38	13.56	−0.96
15	−0.32	11.87	−0.092
16	−0.657	3.10	−0.97
16	−0.156	2.70	−0.10
17	−1.23	12.83	−0.605
17	−0.22	12.58	0.127
18	−3.43	94.03	−0.59
18	−0.57	93.108	0.144

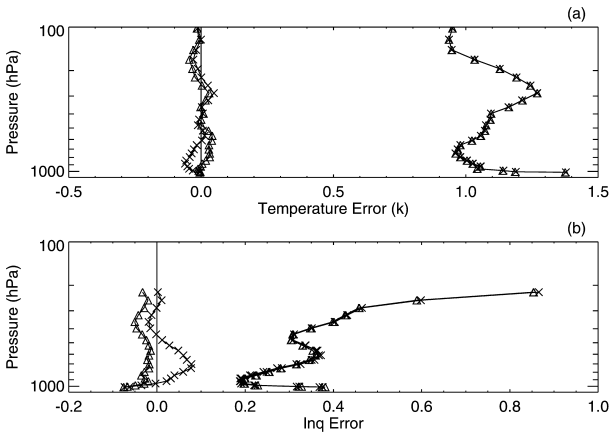

FIG. 8. Temperature and ln$q$ profile retrieval errors for a cloudless true tropical profile for experiment NCA1 (no bias removed, triangles) and NCA3 (bias removed, x signs); (a) bias($T^{sol} - T^{true}$) (left of the figure) and SD($T^{sol} - T^{true}$) on the right (b) Same as in (a), but for ln$q$.

it is assumed that the background error of ln$q$ follows a Gaussian distribution.

Before computing the retrievals, one could remove from the observations the biases computed above as is done in an operational context (e.g., Harris and Kelly 2001). This is done using technique A for experiment NCA3. This experiment is to be compared with NCA1 (bias not removed) and both are illustrated in Fig. 8 for a tropical true profile. The SD of T and ln$q$ hardly changes, but the bias in IWV changes from 0.083 to 2.419 kg m^{-2} (Table 4). The latter is closer to that of IWV^b (3.153 kg m^{-2}). However, a bias in SWS and LWP retrievals has now also been introduced (Table 4). As shown in Fig. 8, removing the bias in T_b has not eliminated the bias of ln$q$ as a function of height. The bias correction changes the mean retrieved value of IWV, while the redistribution of IWV with height is largely controlled by the background error statistics. Only the 150-GHz channel and channels that sample the 183-GHz water vapor absorption line influence the humidity sounding for the tropical profile here in question. Furthermore, the maximum sensitivity as a function of height of the 183-GHz channels to humidity is considerably less than that of the window channels. All of the other humidity sensitive channels are window channels that sense integrated humidity below 500 hPa and, therefore, do not provide much information on its vertical distribution.

4. SSMIS retrievals in cloudy skies

a. Retrievals with technique A

1) IMPACT OF THE SUPERSATURATION CONSTRAINT

Figure 9 illustrates the effect of the SSC in the presence of a cloud for the *U.S. Standard Atmosphere, 1976* true profile. The cloud added to the profile has a LWP of 0.3 kg m^{-2} and is situated between 700 and 750 hPa. The methodology for cloud addition is described in section 2d. The SSC is active for experiment CA6, but not for CA7. The temperature retrievals are not affected by the SSC, because it is assumed that J_{sat} [Eq. (2)] does not depend on temperature. When it is taken into account that J_{sat} depends on temperature, as it in fact does through $q_{sat}(T, p)$, a temperature bias is also present in the solution (not shown here).

The bias of ln$q$ as a function of height is quite different for both experiments. The dry bias in the humidity solution at cloud height is considerable for CA6. Retrievals for both experiments have similar statistics (Table 6). The effect of the SSC is to redistribute the water vapor in the vertical differently, because IWV^{sol} statistics are very similar for the two experiments. This is because of the coarse vertical resolution of the weighting functions for humidity sensitive channels and the fact that the ln$q$ vertical background error correlations are broad. For experiment CA6, the root-mean-square (rms) curve at cloud height is close to the SD curve of CA7 (not shown here). The NCE for the case with SSC active is smaller than for the case where it is inactive, especially at cloud height.

2) EFFECT OF A PRIORI KNOWLEDGE OF CLOUD VERTICAL DISTRIBUTION

The impact of the a priori knowledge of cloud vertical distribution is tested with technique A. For this technique, the CSF (which determines the cloud vertical distribution) is taken from the background cloud and is maintained fixed during the minimization process. If there happens to be no cloud in the background, then a CSF is created as described in appendix A. For technique A, it is assumed that for a given experiment, all samples have the same cloud profile that equals the true

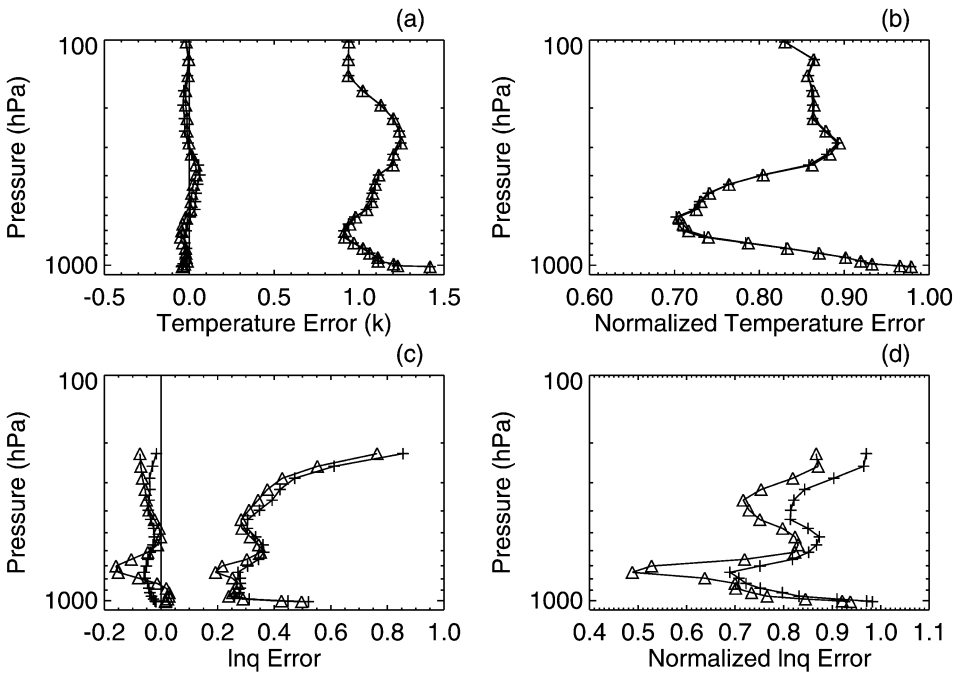

FIG. 9. Effect of the supersaturation constraint. Temperature and ln$q$ profile retrieval errors for a cloudy (Table 6) true *U.S. standard Atmosphere, 1976* profile for experiments CA6 (with SSC) (triangles) and CA7 (without SSC) (plus signs); (a) bias($T^{\text{sol}} - T^{\text{true}}$) left of the figure and SD($T^{\text{sol}} - T^{\text{true}}$) on the right, (b) temperature normalized computed error, (c) same as in (a), and (d) ln$q$ normalized computed errors.

one. Because the LWP background error is set to a large value, a cloud is always allowed to form in the retrieval, but the retrieved LWP varies from one profile to the next, because Gaussian noise is added to the synthetic observations.

To illustrate the impact of the knowledge of the cloud vertical distribution (thus, CSF) using synthetic retrievals, experiments are performed for which the CSF is solely deduced from the background RH (as described in appendix A). This allows the possibility for the cloud to be formed at the wrong vertical position. For these experiments, two different cloud types are chosen: type A with LWP = 0.3 kg m^{-2} situated between 700 and 750 hPa, and type B, with LWP = 0.5 kg m^{-2} situated between 750 and 950 hPa. For experiments with cloud-type A (experiment CA6 = control, and experiment CA8 = test case), retrieval results in Fig. 10 show that when the knowledge of cloud position is erroneous, then very little temperature information can be obtained from the observations. However, retrievals for other variables, such as the ln$q$ profile, IWV, and SWS are only slightly deteriorated (Table 6). For the deeper and heavier cloud case (cloud-type B), the control experiment (CA9) shows that there is a considerable bias in the retrievals of IWV, LWP, and SWS (Table 6). These results are in agreement with those found in Deblonde (2001). The presence of larger values of LWP introduces a bias in the retrievals of IWV and SWS. For the test case where the CSF is not well known a priori (experiment CA10 = test case), the retrievals are affected in a similar way as for the cloud-type A experiment.

For these experiments, without a good a priori knowledge of the cloud vertical distribution, reasonably good retrievals of IWV, ln$q$, and SWS are obtained. This points to the independence between the temperature and remaining variables that constitute the control vector. Thus, although little temperature information is to be expected from retrievals for real observations in cloudy skies with technique A, the retrievals of the other fields are only slightly degraded.

b. Retrievals with technique B

Figure 11 illustrates the retrieval results for experiments with two different cloud types and for a tropical profile. CB12 has a thicker true cloud (750–950 hPa) than CB11 (700–750 hPa) and the LWP values are, respectively, 0.187 and 0.267 kg m^{-2}. The LWP amounts are different from technique A experiments because of the way clouds are generated (section 2d and appendix B). As for the cloudless case, not all sample profiles converge (Table 6). Nevertheless, the solutions statistics for the converging cases are similar to those obtained for technique A (cf. Fig. 10, experiments CA6 and CA8, and those of Fig. 11). However, with technique B, no a priori CSF is provided and yet it is possible to retrieve temperature information even in the presence of clouds (Fig. 11b). This results from the implicit as-

TABLE 6. Bias and SD for $\mathbf{x} - \mathbf{x}^{\text{true}}$ and NCE for experiments with clouds. IWV and LWP: kg m^{-2}, SWS: m s^{-1}, pressure: hPa. Sample size = 3000; BG: background. Northern Hemisphere background error is used for all experiments. For each experiment, top number is bias($\mathbf{x} - \mathbf{x}^{\text{true}}$) and bottom number is SD($\mathbf{x} - \mathbf{x}^{\text{true}}$) as defined in section 2f.

Expt	True profile (No. of diverging cases)	Normalized computed error			IWV		LWP		SWS		Cloud LWP/cloud-top and -bottom pressure
		IWV	SWS	T_{skin}	1DVAR solution	BG	1DVAR solution	BG	1DVAR solution	BG	
CA6	USSD (16)	0.285	0.770	0.979	−0.088	1.281	−0.001	0.000	0.009	−0.031	0.3
					1.092	3.838	0.025		1.537	1.997	700–750
CA7	USSD (0)	0.289	0.766	0.976	0.069	1.295	−0.003	0.000	−0.004	−0.032	0.3
					1.114	3.854	0.025		1.528	1.995	700–750
CA8	USSD (15)	0.300	0.829	1.002	0.124	1.284	−0.004	0.000	0.117	−0.035	0.3
					1.147	3.831	0.026		1.654	1.995	700–750
CA9	USSD (23)	0.215	0.793	0.981	−0.552	1.533	0.011	0.000	0.069	−0.029	0.5
					1.098	5.111	0.031		1.583	1.996	750–950
CA10	USSD (20)	0.221	0.814	0.996	−0.510	1.567	−0.005	0.000	−0.134	−0.034	0.5
					1.141	5.156	0.038		1.622	1.994	750–950
CB11	TROP (541)	—	0.809	0.958	−0.235	−1.390	0.030	2.878	0.145	−0.011	0.267
					1.776	6.509	0.065	3.680	1.615	1.997	700–750
CB12	TROP (711)	—	0.808	0.959	−0.794	−2.804	0.056	3.024	0.151	−0.040	0.187
					1.706	6.184	0.072	3.733	1.619	2.004	700–950

sumption that cloud starts to form when the RH exceeds the preset threshold (95%). This provides some information on the cloud vertical distribution, and thereby allows temperature information to be extracted. The broad vertical resolution of the sensor's weighting functions and the broad background error vertical correlation functions limits the retrieval of cloud vertical distribution. It is not possible to obtain profile information on cloud with a vertical resolution better than that associated with the moisture-averaging kernels (e.g., Rodgers 2000).

Figure 12 illustrates histograms of retrieved LWP for CB11 and CB12. The LWP tends to be overestimated and a few cases have large retrievals of LWP. A lot of these cases again correspond to cases with cloud formation at the surface.

The impact of changing observation error $(\mathbf{E} + \mathbf{F})^{1/2}$ is also investigated for a *U.S. Standard Atmosphere, 1976* true profile with a LWP of 0.39 kg m^{-2} and clouds located between 700–750 hPa. In the first instance, the observation error of the 150-GHz channel and channels sampling the 183-GHz water vapor absorption line observation is reduced by one-half. In the second instance, the same changes as for the first case are implemented, but the error for the window channels 12–18 and the 50.3-GHz temperature channel (also sensitive to q) is also reduced by one-half. The results of these changes do not alter the general conclusions found in this paper.

5. Conclusions

Retrievals using both synthetic background fields and observations are investigated for the SSMIS instrument for clear and cloudy but nonprecipitating conditions over the oceans. The main reasons for using synthetic data are to verify the correctness of the implementation of the 1DVAR scheme and to investigate the behavior of retrievals using a new technique. Also, at this time, the SSMIS instrument is scheduled for launch in the spring of 2003.

Two retrieval techniques are implemented in the 1DVAR and are extensively tested. The control variables for the two techniques are the same (i.e., profile of temperature, surface wind speed, and skin temperature) except for the following: in technique A, profiles of ln$q$ and LWP are control variables and, in technique B, lnq_{total} is a control variable where q_{total} is the sum of q and liquid cloud water content q_L. Functions are also defined that specify how q_{total} is split among its two components, q and q_L. Essentially, excess water vapor oversaturation leads to cloud formation.

First, results are presented for retrievals in cloudless skies (i.e., true cloudless profile). With technique A, it is shown that the normalized computed error is close to the normalized theoretical error (obtained from the Hessian) for temperature retrievals (close to linear problem) and is quite different for ln$q$ because of the nonlinear dependence of the forward operator on ln$q$ and the use

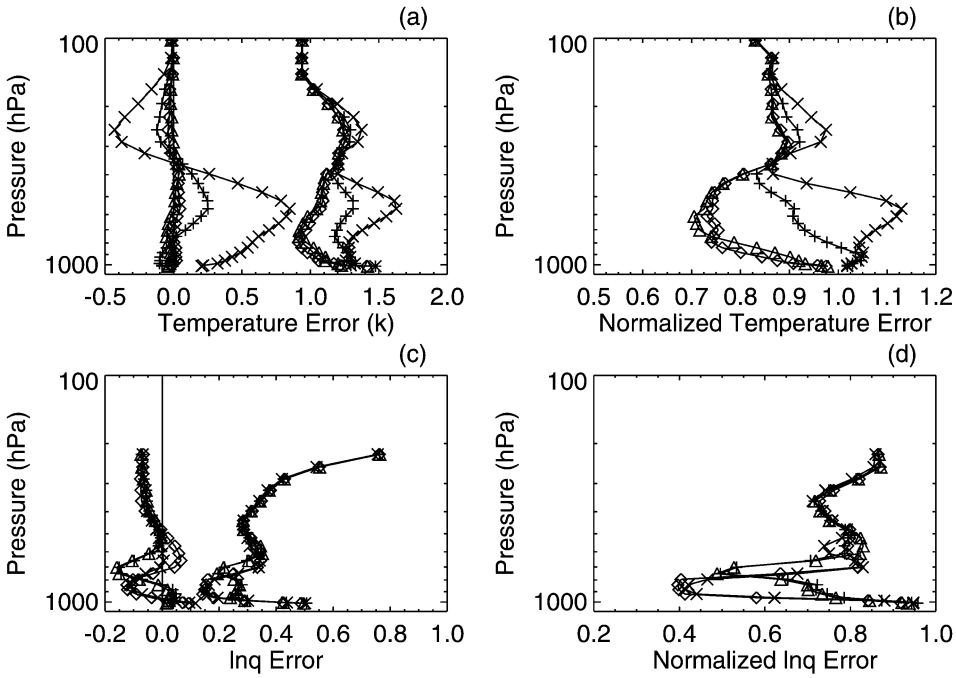

FIG. 10. Effect of knowledge of a priori cloud vertical distribution. Temperature and ln$q$ profile retrieval errors for a cloudy true *U.S. Standard Atmosphere, 1976* profile for experiments CA6 (triangles) and CA9 (diamonds) (both with CSF taken from background cloud), and CA8 (plus signs) and CA10 ($\times$ signs) (both with CSF computed from background RH). LWP and cloud location are given in Table 6. (a) Bias($T^{\text{sol}} - T^{\text{true}}$) and SD($T^{\text{sol}} - T^{\text{true}}$) on the right, (b) temperature normalized computed error, (c) same as in (a), and (d) ln$q$ normalized computed errors.

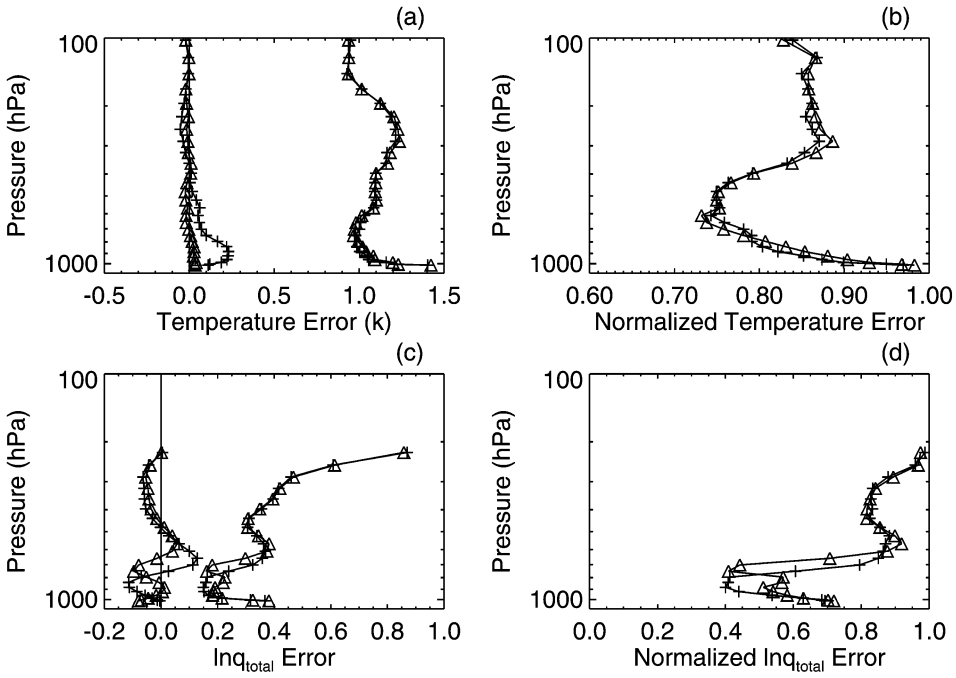

FIG. 11. Same as in Fig. 9, but for experiments CB11 (triangles) and CB12 (plus signs). The true profile is the tropical profile. Each experiment has a different type of cloud (Table 6).

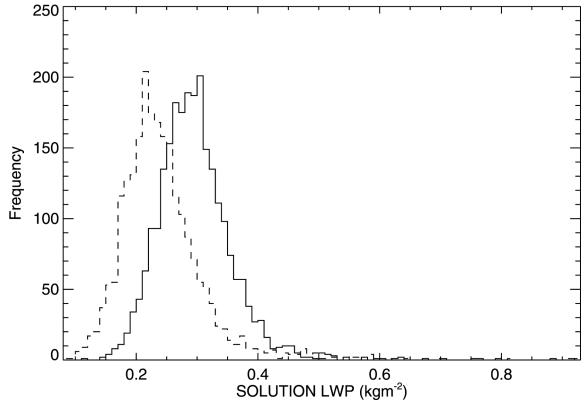

FIG. 12. Histograms of cloud liquid water path (kg m^{-2}) for experiments CB11 (continuous line) and CB12 (dashed line).

of a supersaturation constraint. The accuracy of the LWP retrievals (true value of zero) is as expected and a symmetric distribution of LWP (negative and positive values) is obtained around the true value of zero. Retrievals with technique B (which implicitly includes a SSC because excess water vapor goes into cloud formation) are similar to those of technique A, except that LWP retrievals are positive only by construction and tend to be slightly overestimated. The number of diverging cases is also shown to be much larger.

The cause of the solution biases for the vertical distribution of humidity is also discussed. Part of the bias is shown to be attributable to the choice of moisture control variable for which the background error is assumed to follow a Gaussian distribution. However, because of the different dependence of T_b on q for the humidity sounding (more linear in ln$q$) and window channels (more linear in q), the choice of control variable that reduces the nonlinearity of the forward model, to in turn also minimize the biases in the humidity solution, is by no means straightforward.

Second, results are presented for retrievals in cloudy skies (true profile is cloudy). With technique A, it is shown that the supersaturation constraint introduces considerable biases in humidity at cloud height due to the broadness of both the humidity sensitive weighting functions and vertical correlation of ln$q$ background error. It is also shown that little temperature information (except well above the clouds) can be extracted if the a priori cloud vertical distribution is not well known. However, technique B allows for some temperature retrieval from the observations even in the presence of clouds because it has some skill at positioning the cloud. This is the main advantage of using technique B. This comes at a cost, though, by considerably increasing the number of iterations before convergence of the minimization problem is reached, and a considerable number of cases do not converge.

Acknowledgments. The SSMIS 1DVAR code was developed while the first author was a visiting scientist at the Met Office. The additional costs of this visit were met by the EUMETSAT-funded Satellite Application Facility for Numerical Weather Prediction. The authors thank Sean Healy (Met Office) for providing his implementation of the Levenberg–Marquardt minimization scheme and for several fruitful discussions, and John Eyre (Met Office) for his comments on the paper. The authors also appreciate the insight provided by Mark Buehner (Meteorological Service of Canada) on the topic presented in section 3c.

APPENDIX A

Cloud Structure Function: No Clouds in the Background Field

If $\mathrm{LWP}^b = 0.0$, then a nonzero cloud structure function (CSF) is generated where RH of the background profiles (RH^b) exceeds a preset threshold value RH_T (e.g., 80%). First a variable C_i is defined that indicates presence or absence of cloud at level i:

$$C_i = \begin{cases} 1 & \text{if } \mathrm{RH}_i^b \geq \mathrm{RH}_T, \\ 0 & \text{if } \mathrm{RH}_i^b < \mathrm{RH}_T. \end{cases} \tag{A1}$$

Then a normalizing factor N_O is computed:

$$N_O = \frac{1}{g} \sum_{i=1}^{N_p} \Delta p_i C_i, \tag{A2}$$

where Δp_i is the pressure difference between two levels, N_p is the total number of pressure levels, and CSF is

$$\mathrm{CSF}(p_i) = C_i / N_\mathrm{o}. \tag{A3}$$

If there is still no cloud (in the case of a dry background cloud profile for example), then a nonzero CSF is assigned to levels in the lower troposphere as follows:

$$C_{L-i} = 1;\ i = 3, 4, 5, \tag{A4}$$

where L is the index of the lowest pressure level. This implies that clouds cannot be formed for levels C_L, C_{L-1}, and C_{L-2} (i.e., at and close to the surface). Note that $C_i = 0$ if $T < 253$ K. Thus, it is assumed that supercooled water can not be present for $T < 253$ K.

APPENDIX B

Splitting of q_{total} into q and q_L

Define $\mathrm{RH}_{q\mathrm{total}} = q_\mathrm{total}/q_\mathrm{sat}$; then q depends on q_total as follows:

$\mathrm{RH}_{q\mathrm{total}} < \mathrm{RH}_1$:

$$q = q_\mathrm{total}$$

$\mathrm{RH}_2 > \mathrm{RH}_{q\mathrm{total}} \geq \mathrm{RH}_1$:

$$q = \mathrm{RH}_1 q_\mathrm{sat} + C_\mathrm{split}(q_\mathrm{total} - \mathrm{RH}_1 q_\mathrm{sat})$$

$\mathrm{RH}_{q\mathrm{total}} \geq \mathrm{RH}_2$:

$$q = q_\mathrm{sat}[\mathrm{RH}_1 + C_\mathrm{split}(\mathrm{RH}_2 - \mathrm{RH}_1)], \quad \text{and} \tag{B1}$$

$$q_L = q_\mathrm{total} - q. \tag{B2}$$

Thus, once $RH_{q\text{total}}$ reaches a threshold of RH_1, the excess of q_{total} over $RH_1 q_{\text{sat}}$ is split among q and q_L. When $RH_{q\text{total}}$ exceeds RH_2, then q remains fixed and the excess is taken by q_L. In this paper, $RH_1 = 0.95$, $RH_2 = 1.05$, and $C_{\text{split}} = 0.5$.

The derivatives of T_b with respect to $\ln q_{\text{total}}$ and temperature (T) are

$$\frac{\partial T_b}{\partial \ln q_{\text{total}}} = q_{\text{total}} \frac{\partial T_b}{\partial q_{\text{total}}}$$

$$= q_{\text{total}} \left(\frac{\partial T_b}{\partial q} \frac{\partial q}{\partial q_{\text{total}}} + \frac{\partial T_b}{\partial q_L} \frac{\partial q_L}{\partial q_{\text{total}}} \right) \text{and} \quad \text{(B3)}$$

$$\frac{\partial T_b}{\partial T} = \frac{\partial T_b}{\partial q} \frac{\partial q}{\partial q_{\text{sat}}} \frac{dq_{\text{sat}}}{dT} + \frac{\partial T_b}{\partial q_L} \frac{\partial q_L}{\partial q_{\text{sat}}} \frac{dq_{\text{sat}}}{dT}. \quad \text{(B4)}$$

APPENDIX C

Computation of Simulated Background Profiles

Simulated background fields $\mathbf{x}_j^b$ ($j = 1, N$, where N is the sample size taken to be 3000 in this study) are obtained following Rodgers (2000) and are computed as follows:

$$\mathbf{x}_j^b = \mathbf{x}^{\text{true}} + \boldsymbol{\varepsilon}_j, \quad \text{(C1)}$$

where $\mathbf{x}^{\text{true}}$ is the selected true profile and $\boldsymbol{\varepsilon}_j$ is noise vectors computed from the eigenvectors and eigenvalues of the background error covariance matrix $\mathbf{B}$ (see, section 2e). Here, $\mathbf{B}$ can be written as

$$\mathbf{B} = \sum_{i=1}^{N_c} e_i \mathbf{F}_i \mathbf{F}_i^{\mathrm{T}}, \quad \text{(C2)}$$

where N_c is the dimension of the control vector $\mathbf{x}$, and e_i and $\mathbf{F}_i$ are, respectively, the eigenvalues and eigenvectors of $\mathbf{B}$. The eigenvalues are equal to the background error variances, which are the diagonal elements of $\mathbf{B}$. The noise vector for each member of a random sample of size N is

$$\boldsymbol{\varepsilon}_j = \sum_{i=1}^{N_c} a_{i,j} e_i^{1/2} \mathbf{F}_i, \quad \text{(C3)}$$

where $a_{i,j}$ is a random number drawn from a Gaussian distribution with zero mean and unit standard deviation.

APPENDIX D

Computation of $T_b^o - T_b(\mathbf{x}^b)$

The distribution of $T_b^o - T_b(\mathbf{x}^b)$ when the background error of q is assumed Gaussian is computed as follows. First, the background error covariance matrix for q is computed from that of $\ln q$. This is done by computing an ensemble of deviations δq with respect to a given true profile q^{true}.

$$\delta q = q^{\text{true}}(e^{\delta \ln q} - 1), \quad \text{(D1)}$$

where $\delta \ln q$ are elements of noise vectors obtained as in Eq. (C1). Second, noise vectors for q with a Gaussian distribution are computed as in section 2d, but the background error covariance matrix used is that of q and not $\ln q$. Last, $T_b^o - T_b(\mathbf{x}^b)$ is computed.

REFERENCES

Alishouse, J. C., J. B. Snider, E. R. Westwater, C. T. Swift, C. S. Ruf, S. A. Snyder, J. Vongsathorn, and R. R. Ferraro, 1990: Determination of cloud liquid water content using the SSM/I. *IEEE Trans. Geosci. Remote Sens.,* **28,** 817–822.

Blankenship, C. B., A. Al-Khalaf, and T. T. Wilheit, 2000: Retrieval of water vapor profiles using SSM/T-2 and SSM/I data. *J. Atmos. Sci.,* **57,** 939–955.

Bommarito, J., 1993: DMSP Special Sensor Microwave Imager Sounder. *Proc. SPIE,* **1935,** 230–238.

Deblonde, G., 2001: Variational retrievals using SSM/I and SSM/T-2 brightness temperatures in clear and cloudy situations. *J. Atmos. Oceanic Technol.,* **18,** 559–576.

——, and S. J. English, 2000: Evaluation of the FASTEM2 fast microwave oceanic surface emissivity model. *Tech. Proc. 11th Int. ATOVS Study Conf.,* Budapest, Hungary, Bureau of Meteorology Research Centre, 67–78.

English, S. J., 1999: Estimation of temperature and humidity profile information from microwave radiances over different surface types. *J. Appl. Meteor.,* **38,** 1526–1541.

——, and T. J. Hewison, 1998: A fast generic millimeter-wave emissivity model. *Proc. SPIE,* **3503,** 288–300.

Eyre, J. R., 1989: Inversion of cloudy satellite sounding radiances by nonlinear optimal estimation. I: Theory and simulation for TOVS. *Quart. J. Roy. Meteor. Soc.,* **115,** 1001–1026.

——, 1991: A fast radiative transfer model for satellite sounding systems. ECMWF Tech. Memo. 176, 28 pp. [Available from ECMWF, Shinfield Park, Reading, Berkshire RG2 9AX, United Kingdom.]

——, and A. D. Collard, 1999: The effects of non-linearity on retrieval errors: Implications for the interpretation of advanced infra-red sounder data. *Tech. Proc. 10th Int. TOVS Study Conf.,* Boulder, Colorado, Bureau of Meteorology Research Centre, 191–202.

Gérard, E., and R. W. Saunders, 1999: Four-dimensional assimilation of special sensor microwave/imager total column water vapor in the ECMWF model. *Quart. J. Roy. Meteor. Soc.,* **125,** 3077–3101.

Greenwald, T. J., G. L. Stephens, T. H. Vonder Harr, and D. L. Jackson, 1993: A physical retrieval of cloud liquid water over the global oceans using SSM/I observations. *J. Geophys. Res.,* **98,** 18 471–18 488.

Harris, B. A., and G. Kelly, 2001: A satellite radiance-bias correction scheme for data assimilation. *Quart. J. Roy. Meteor. Soc.,* **127,** 1453–1468.

Liebe, H. J., 1989: MPM—An atmospheric millimeter wave propagation model. *Int. J. Infrared Millimeter Waves,* **10,** 631–650.

——, P. W. Rosenkranz, and G. A. Hufford, 1992: Atmospheric 60 GHz oxygen spectrum: New laboratory measurements and line parameters. *J. Quant. Spectros. Radiat. Transfer,* **48,** 629–643.

Lorenc, A. C., 1986: Analysis methods for numerical weather prediction. *Quart. J. Roy. Meteor. Soc.,* **112,** 1177–1194.

Petty, G. W., and K. B. Katsaros, 1994: The response of the SSM/I to the marine environment. Part II: A parameterization of the effect of the sea surface slope distribution on emission and reflection. *J. Atmos. Oceanic Technol.,* **11,** 617–628.

Phalippou, L., 1996: Variational retrieval of humidity profile, wind speed and cloud liquid-water path with the SSM/I: Potential for numerical weather prediction. *Quart. J. Roy. Meteor. Soc.,* **122,** 327–355.

Press, W. H., B. P. Flannery, S. A. Teukolsky, and W. T. Vetterling, 1986: *Numerical Recipes.* Cambridge Press, 818 pp.

Rodgers, C. D., 2000: *Inverse Methods for Atmospheric Sounding: Theory and Practice*. World Scientific, 238 pp.

Rosenkranz, P. W., 2001: Retrieval of temperature and moisture profiles from AMSU-A and AMSU-B measurements. *IEEE Trans. Geosci. Remote Sens.*, **39,** 2429–2435.

Saunders, R. W., M. Matricardi, and P. Brunel, 1999: An improved fast radiative transfer model for assimilation of satellite radiance observations. *Quart. J. Roy. Meteor. Soc.*, **125,** 1407–1425.

Swadley, S. D., and J. Chandler, 1991: The defense meteorological satellite program's Special Sensor Microwave Imager/Sounder (SSMIS). Preprints, *Seventh Symp. on Meteorological Observations and Instrumentation*, New Orleans, LA, Amer. Meteor. Soc., 175–178.

Wilheit, T. T., 1990: An algorithm for retrieving water vapor profiles in clear and cloudy atmospheres from 183 GHz radiometric measurements: Simulation studies. *J. Appl. Meteor.*, **29,** 508–515.